Microelectronic Engineering 87 (2010) 652–657

Contents lists available at ScienceDirect

Microelectronic Engineering

journal homepage: www.elsevier.com/locate/mee

Silicon nanostencils with integrated support structures

Shawn Fostner [a,*], Sarah A. Burke [b], Jessica Topple [a], Jeffrey M. Mativetsky [c], Jean Beerens [d], Peter Grutter [a]

[a] Physics Department, McGill University, 3600 Rue University, Montreal, QC, Canada H3A 2T8
[b] Department of Physics, University of California at Berkeley, Berkeley, CA 94720-7300, USA
[c] Institut de Science et d'Ingénierie Supramoléculaires (ISIS) CNRS 7006, Université de Strasbourg, 8 Allée Gaspard Monge, 67000 Strasbourg, France
[d] Centre de Recherche en Nanofabrication et Nanocaractérisation, Département de génie électrique et de génie informatique, Université de Sherbrooke, Sherbrooke, QC, Canada J1K 2R1

ARTICLE INFO

Article history:
Received 9 December 2008
Received in revised form 20 July 2009
Accepted 4 September 2009
Available online 9 September 2009

Keywords:
Silicon stencil
Pattern transfer
Tantalum film
Nanostructuring
Film stress
MEMS
Stabilization structures
Stencil deformation

ABSTRACT

We describe the fabrication of single crystal silicon membranes for stencil mask deposition. The membranes are created using standard microfabrication techniques combined with focussed ion beam milling to give structures with openings hundreds of micrometers to 50 nm in size. Deflection of the membrane structures under the deposition of highly stressed metals films is measured for vacuum deposited tantalum films, and used to estimate a film stress of 1.3 ± 0.1 GPa. In order to overcome these significant deflections, we have integrated simple stiffening structures into the membranes themselves which both preserve line of sight to the sample as well as provide a sufficiently large bending moment to resist vertical deflections which would otherwise cause noticeable feature broadening. Deposition of metallic nanowires on the surface shows good agreement with the calculated and measured deflections of the reinforced structures.

1. Introduction

The quest to control the size and functionality of devices at ever smaller scales has been an area of significant research and development over the past decades. Lithographic processing for device fabrication and research has made significant progress in recent years in terms of complexity, size of features, and potential materials. However, most techniques are geared towards the bulk processing of semiconductor wafers in ambient environments, and involve wet processing and stringent material restrictions. Stencil masks are an attractive alternative which use a wide range of nanometer to micrometer openings on a thin stencil within close proximity of a surface to mask physical deposition of a wide range of evaporants on arbitrary substrates. As a result, it is possible to deposit on sensitive substrates such as alkali halides under ultrahigh vacuum (UHV) conditions. This leads to the possibility of measurements on structures of well defined chemical composition even at an atomic scale. Numerous examples of nanostencils have been published using silicon nitride membranes [1–6], cantilever based masks [7,8], and silicon on insulator membranes [9]. Stencils have also been demonstrated in dynamic modes, using AFM cantilevers or mask manipulation *in-situ* to position apertures relative to the sample [4,5,7,8], and static modes [1,2,6,3,9] with a prefabricated stencil which is clamped directly to the sample.

The primary limitation of silicon nitride based masks lies in creating as low stress a membrane as possible in order to avoid catastrophic failure of the mask, either during manufacture or deposition. In addition, there is the added difficulty of ensuring that the mask maintains its shape during deposition as the deposited layers can cause deformation of the membrane depending on the stiffness of the mask and the stress in the deposited layer. There have been recent efforts to create stabilizing structures using silicon nitride masks that are either corrugated or supported by large silicon support frames nearby [10–12] in order to maintain feature size and fidelity during the deposition of high thickness and high stress films. The principle limitation of these techniques is the deformation of the thin membrane near the opening as a result of the trade-off between the size of the support structures and the line of sight between the source and substrate. Large support frames, required to resist significant deformation when using thin membranes, need to be further from the openings in order to avoid occluding the beam of evaporated material.

An alternative is to use bulk silicon membranes to create the masks, thereby avoiding the problems of inherently stressed membranes such as silicon nitride, but requiring careful thinning of the membranes to achieve acceptable thicknesses. We describe here an all silicon stencil with features as small as 50 nm in conjunction

* Corresponding author.
E-mail address: sfostner@physics.mcgill.ca (S. Fostner).

0167-9317/$ - see front matter © 2009 Elsevier B.V. All rights reserved.
doi:10.1016/j.mee.2009.09.004

with micron scale features as long as 200 μm. The mask is suspended in a silicon frame up to a cm across and is created using bulk silicon microfabrication and focussed ion beam milling (FIB) to create both the nanometer and micrometer features. Unlike typical silicon nitride membranes or even silicon on insulator films, the absence of a deposited layer largely circumvents the issue of inherent stress in the membrane and allows for thick silicon membranes which can then be subsequently thinned to smaller active areas. The membrane regions range from 100 μm up to several millimeters, with thicknesses of 0.5–2 μm. Before machining the stencil using the FIB, the membranes are further thinned using a reactive ion etch process to less than 1 μm. The deformation and improvements of silicon structures with integrated silicon supports will be discussed.

2. Stencil fabrication

We fabricate the membranes from N type, 1–10 Ω cm, double side polished 6 in. silicon wafers with a thickness of 610–640 μm. The wafers are first thermally oxidized in a wet ambient to 5000 Å. An EVG 620 aligner and SiteCoat Spin-Coater is used for patterning and exposure. The wafers are etched in 25% tetramethylammonium hydroxide (TMAH) at 85 °C. The back side openings for the membranes are created using either 1.5 mm or 2 mm openings along the (1 1 0) wafer directions, which give membranes 750 μm or 1.25 mm wide, with slight variations depending on the precise ratio of (1 1 1) to (1 0 0) etch rates for a given solution. In order to control the membrane thickness, a simple timed etch is used. It should be noted that various etch stop techniques are viable methods of halting the silicon etch and controlling the membrane thickness more accurately but in practice are either unnecessary or undesirable here, often requiring heavy doping of the silicon surface resulting an implied inherent stress introduced into the membrane. As well, the thickness control of direct wet etching is sufficient to within several micrometers, with subsequent thinning as described below. The wafers are initially dipped in 10% HF for 30 s to remove any environmental oxide, then etched immediately in TMAH for 2.5 h. The etch depth is then carefully measured using a profilometer in multiple points across each wafer to assess the exact solution etch rate. A final etch time is calcu-

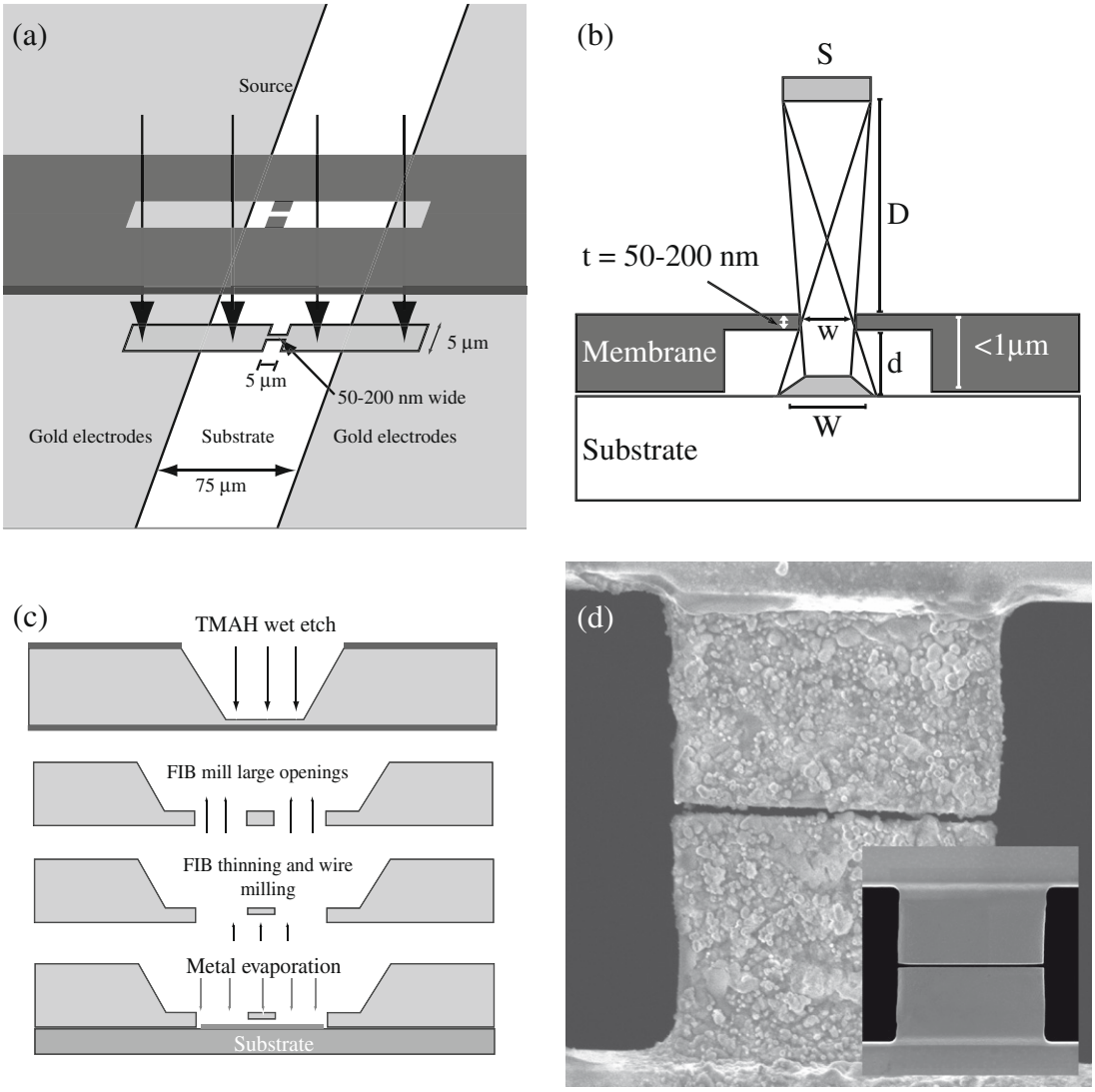

Fig. 1. (a) Schematic of the stencil alignment with a sample possessing two macroscopic contact pads. (b) Broadening of the deposited features due to the geometric limitations of the setup. The thinned membrane, *t*, is spaced from the sample position by up to a micron, typically. (c) Side view of the membrane in a simplified process flow. The suspended region represents the central thinned part of the membrane. (d) Heating the FIB milled silicon sections in air for 10 min at 100–150 °C produced significant deformaties (blisters or bubble-like structures) of the exposed silicon areas as shown. The number of deformities in some cases is even more severe than shown but is present only in FIB machined sections. Inset: a pristine stencil.

lated based on the measured wafer thickness. Wafers are removed at that point and checked by eye, and if necessary re-etched for short periods.

The membrane thickness, which is typically 1–10 μm after the initial silicon etch, is fine tuned by placing it in a reactive ion etcher to reduce the overall thickness to less than 2 μm. Optical observation is typically sufficient to estimate the thickness to within one micrometer. Placing the silicon membrane in the FIB, both micrometer and nanometer size features are then milled as shown in Fig. 1c. A dual beam FIB, Zeiss 1540 XB, is used to create openings in the membrane, which are then measured using the SEM at a tilt angle of 54°. In order to perform electrical measurements using the wires deposited using these stencils, we create two large openings through the membrane 50–100 μm in length which are separated by 5 μm as shown in Fig. 1a. To bridge these two openings, the region between them is thinned to the order of 50–200 nm and an opening from 50–200 nm is milled, with an aspect ratio of local membrane thickness to line width of less than 2. The thickness of this region is designed to be similar to the width of the slit, such that shadowing effects due to the aspect ratio of the mask do not dominate during deposition [3]. If desired, both higher and lower aspect ratios are readily possible. For membranes with the staircase structure, shown in Fig. 2 and described below, the thinning process with the FIB takes several steps but the result is similar in the central region. Milling of the large openings and the thinning process both take place at 2 nA beam currents, while the final narrow line is created using a beam from 5 to 50 pA depending on the precise width required. This has the effect of creating two macroscopic openings with a single thin opening for depositing both contact pads and an integrated wire in a single step.

After fabricating the stencils, we recommend that one avoids heating the chips in air while attaching or handing them. It was found that heating as low as 100° in air for several minutes caused the formation of bubbles and small blisters on the surface of the thin 50–100 nm regions in the center of the membrane, shown in Fig. 1d. These deformities were sufficient to cause the small stencil openings to close, rendering them unusable. It was found that heating under low or ultra high vacuum to remove surface adsorbates did not cause the same problem, even at higher temperatures (150 °C) and over extended periods as long as 7 h, corresponding to the baking time for the mask in the vacuum chamber before use. As the changes are only present in regions of the mask which have been exposed to the gallium beam during FIB, we speculate these features are a result of the diffusion of gallium out of the FIB region. It is not understood why this effect is observed only in air, as baking in both ovens and in the chamber itself should ensure similar temperatures. That this occurs only in the presence of oxygen suggests the possibility of oxidation effects. This is supported by the presence of nearly perfect circular bubbles on the surface which are similar to those found during the gallium catalyzed growth of silicon oxide wires and nodules on a silicon surface usually observed at higher temperatures [13].

3. Deposition characteristics

Producing features on the sample which accurately reproduce the stencil dimensions relies critically on the spacing between the sample and stencil mask. Given the dimensions shown in Fig. 1b, it is apparent from geometric considerations that the width of the deposited features is $W = w + \frac{d}{D}S$, where w is the stencil opening size, d the spacing between sample and mask, D the source to mask spacing, and S the size of the source. In this case, because the nanoscale features are recessed from the sample surface, there is unavoidable spreading in the deposited features. For a 2 mm source at a distance of 10 cm with a spacing of 1 μm, the spreading should be limited to 20 nm, provided surface diffusion of the adsorbates is not a significant factor. Similarly, there is a reduction in the feature size at the top of the deposited structure by the same fraction. This results in a diffuse edge to the deposited wires [14].

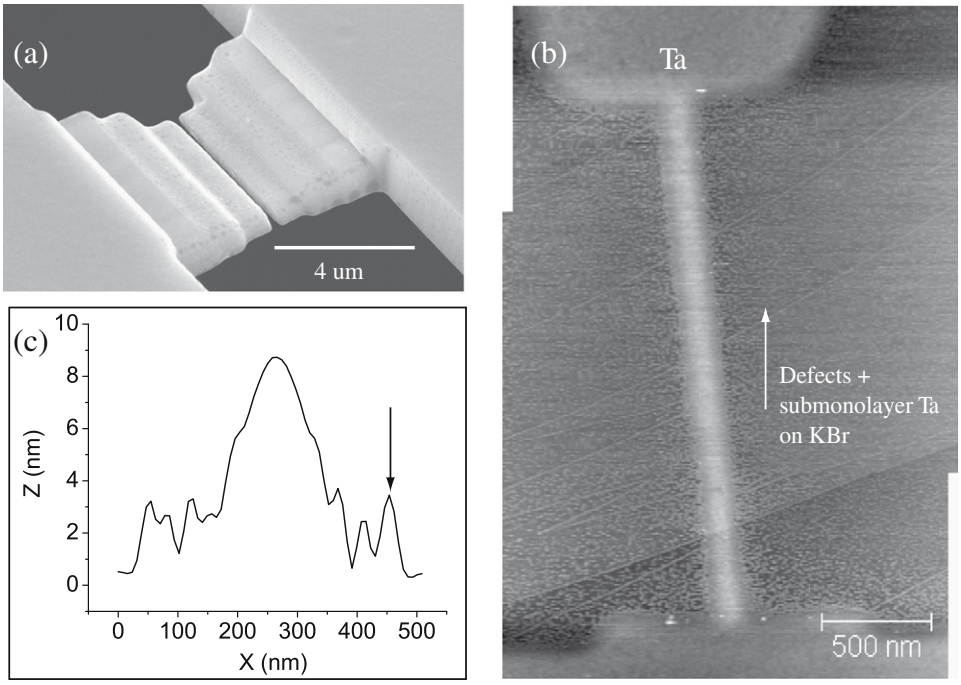

Fig. 2. Silicon membranes with the FIB thinning in a staircase sequence to improve the membrane stability against deformation. (a) Angled SEM image of the thinned membrane, the sample would be approached to the stencil from above in this image. (b) 11.5 nm tall Ta film deposited on KBr through the same mask with a 150 nm wide opening (wire heights are often slightly smaller as shown, but range from 8.5 to 11 nm high along the wire depending on the grains present) and imaged in UHV using tapping mode AFM. (c) Line profile (smoothed) of the deposited wire trace, with a width of 170 nm. Peaks beside the main feature, indicated in both the line scan and afm image by arrows, are not noise but are reproducible particles and defects formed by a shadow of diffusing submonolayer particles well outside the range of the geometric shadow given by the deposited line [14].

The advantage of this procedure is that the mask itself can be in contact with the sample, but has a known spacing d to the critical 50–200 nm opening which is protected from damaging contact with the sample itself. To avoid this feature enlargement, it is possible to perform the milling process from the back side of the wafer, thereby allowing better contact with the sample but with a consequently greater risk to the stencil.

Using an electron-beam evaporator (Oxford Applied Research), we deposited tantalum films onto a substrate under ultra high vacuum through these stencils. Deflections of the silicon beams forming the nanowire gap are clearly visible with film thicknesses of 45 nm as shown in Fig. 3b. The degree of deflection varied over a single chip due to variations in the exact thickness and lengths of the silicon beams.

In order to understand the bending, the deflection and radius of curvature were measured and used to estimate the tantalum film stress using the modified form of Stoney's formula [15]

$$\sigma = \frac{E t_{sub}^2}{6 R t_{film}(1-\nu)} \tag{1}$$

where σ is the film stress, E is Young's modulus of the silicon substrate, t_{sub} is the beam thickness, R is the radius of curvature of the beam, t_{film} is the film thickness, and ν is Poisson's ratio for silicon. A ratio of $\frac{E}{(1-\nu)} = 180.5$ GPa was used [16] for E and ν. We can also write this in terms of the bending moment of the thin rectangular section,

$$\sigma = \frac{2EI}{R t_{film} t_{sub} b (1-\nu)} \tag{2}$$

with b the width of the beam, as in the horizontal direction in Fig. 1c, where the moment $I = \frac{b t_s^3}{12}$. For cases of small bending it is also possible to substitute $R = \frac{l^2}{2\delta}$ where l is the beam length, and δ is the deflection at the end of the beam.

The film thickness t_{film} was measured using a quartz crystal microbalance (Inficon) to calculate the rate before and after deposition, with typical rates of 0.3–0.5 Å/min. Metal films were evaporated on the back side of the beam, opposite the thinning direction as shown in Fig. 3b and d. The primary source of error in the measurement of the film stress lies with the thickness of the silicon beams themselves, not the deposited film thickness. The thickness of the FIB thinned sections, from 110 to 220 nm ± 5–30%, was estimated from an angled SEM image. This was limited by the poor edge contrast of the thin sections, as well as rounding of the edge due to edge enhanced milling by the ion beam. The variation results from the thinning process in the FIB as well as local thickness variations in the silicon membrane. In the case shown in Fig. 3a tantalum film with a total thickness of 45 nm was deposited in a series of smaller depositions of 5–10 nm onto silicon beams with a mean beam thickness of 165 nm ± 15%, and then imaged using the SEM.

We should note that Stoney's equation is most accurate for film thicknesses much smaller than the substrate. In our case, the deposited film can be as much as 40% of the substrate thickness so corrections to the calculated film stress are called for. Klein [17] has shown that the stress value is overestimated by a fraction ϵ given by the thickness and modulus ratio of film to substrate, δ, and γ.

$$\epsilon_{st} = \frac{\delta(1-\gamma\delta^2)}{1+\gamma\delta^3} \tag{3}$$

The modulus for Ta on (1 0 0) silicon is taken to be 175 GPa [18], with the other parameters as given above. Taking into account this correction we have calculated a film stress of 1.3 ± 0.1 GPa based

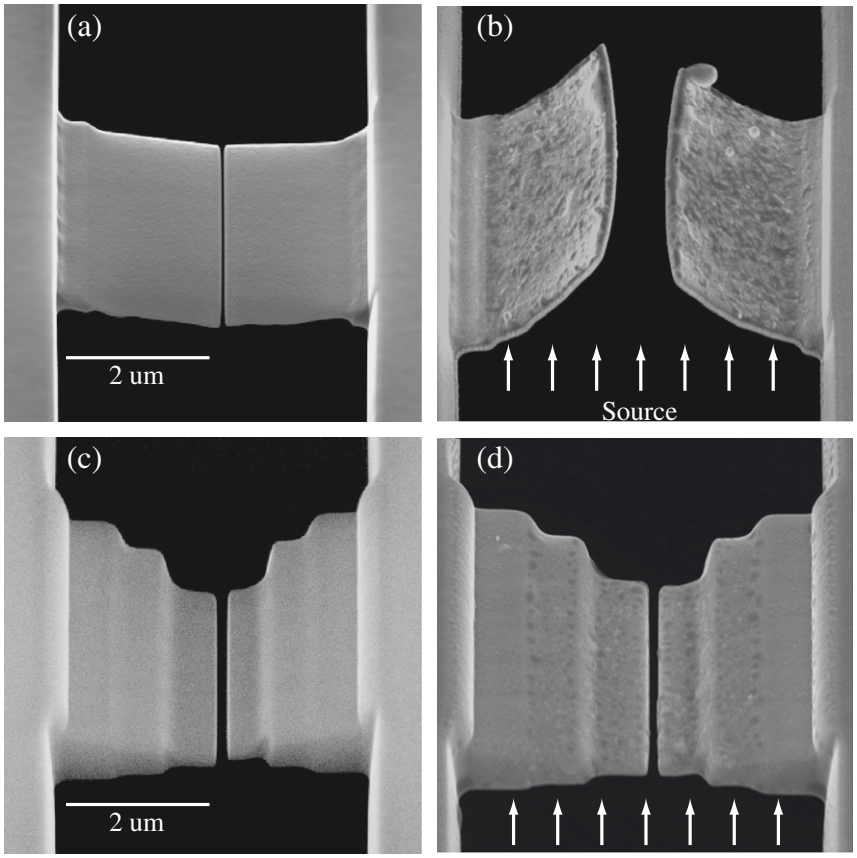

Fig. 3. A comparison of the membrane deflection of reinforced and normal membrane structures with Ta films deposited on the backside. (a) and (b) Uncompensated structure, with significant vertical deflection and 45 nm Ta. (c) and (d) Reinforced structure under 27 nm Ta film thickness and no visible deflection.

on the measured beam radii, which is consistent with measured stress values for tantalum thin films deposited on bulk silicon wafers [19]. The previous tantalum film measurements were not given for thicknesses this low, but extrapolating the film stress from Guisbier's published data is consistent with our film stress. The measured membrane deflections range from 0.6 to 1.4 μm, with an average beam length of 2.5 μm, and thicknesses of 110–220 nm. This deflection is larger than that predicted based on the radial curvature and these stress values but is a result of the non uniform curvature at the corners as well as a zero offset in the deflection as measured from the fixed end. For this reason the measured radii were used over static deflections.

The beam deflections observed are sufficient to cause a significant increase in the deposited wire thickness over the course of several deposition cycles, well before the advent of clogging due to evaporated materials. If we are dealing with a metal with a well known surface stress we could even design the thickness of the beam to deliberately destort just enough that the gradual distortion will prevent the complete closure of the gap. In practice this would be difficult and would require advance knowledge of the film stress for the materials involved, but would be a way to prolong the lifespan of small aperture openings despite large deposition thicknesses. This mechanism may already take place inadvertently in some stencil depositions.

In order to avoid the effects of this undesirable distortion with such high stress films, it is possible to design the profile of the membrane to increase the bending moment of the silicon substrate. For nitride stencils, this has been shown through the use of corrugated membranes [11,12] and silicon supported structures [10]. The advantage in the method proposed here is that the supporting structures exist as a part of the membrane itself and as a result can be tailored to fit the application with minimal limitations on size and proximity. The changes in the fabricated membrane are shown in Fig. 2a. While the final thickness of the beams close to the opening remains the same, the membrane thickness is increased sequentially outwards from this point. The staircase structure shown is a compromise in terms of effective stiffening and the machining difficulty, as a smoothly sloping structure is similar in concept but is more difficult to physically manufacture with the FIB.

The magnitude of the bending was calculated in order to find the optimal height of the steps and lengths in the staircase for designing these staircase structures. We assume that each step in the staircase represents a beam in its own right, with a slightly different radius of curvature. By aligning the segments and their slopes at each point to create a continuous structure we can estimate the bending. As the curvature is dependent on the square of the substrate thickness, only the thinnest segments will have a significant effect on the deflection. There is a great deal of flexibility in the choice of final thickness, gap size, number of steps, and the height and length of each step. We are constrained by line of sight limitations given by the angle of the sample with respect to the source normal which also limits the aspect ratio of the gap width to the thickness of the final segment, both of which are dependent on the source size, distance, and mask mounting procedure. For the structure shown in Fig. 3c we calculate an approximate vertical deflection of 46 and 40 nm for the left and right segments, respectively. This gives more than an order of magnitude less vertical deflection than the unsupported case, and an even smaller increase in the gap size horizontally, on the order of nanometers or less. By comparison, a single 100 nm beam with a length of 2.5 μm would give a deflection on the order of 400–500 nm and an increase in the gap size of tens of nanometers.

Two membrane openings with both the original and staircase structures are shown in Fig. 3. The width of the final segment in this structure is 100 ± 20 nm, and is the smallest of the beams on the membrane hence the most susceptible to significant deflections under stress. The deposited film thickness in the two cases are 45 and 27 nm for the original (a) and staircase (c) structures, respectively. While a significant deflection in the original feature is observed, shown in Fig. 3b, the staircase structure (d) shows no visible deflection. Deflections less than several tens of nm are difficult to detect. In comparison to the original structures with a similar final thickness, the distortion is more than an order of magnitude smaller, consistent with the projected deflection above. Repeated use of the same mask for a significant number of evaporations and more than 100 nm of deposited tantalum was found to have no visible effect on the deflection, though at this point clogging of the wire gap is beginning to become an issue.

An example of a masked structure is shown in Fig. 2b and c. The image was taken using a JEOL 4500a atomic force microscope (AFM) in UHV with tapping mode over two separate images, due to a limited scan range. An 11.5 nm tantalum film was deposited through the stencil onto a KBr insulating surface under UHV with the membrane in direct contact with the sample surface. The stencil thickness is 1200 ± 50 nm with a wire size of 150 ± 5 nm. The deposited wire size was 180 ± 20 nm. From the geometric spreading discussed above this gives a mask to sample spacing of 900 ± 600 nm which is consistent with the mask to sample spacing d in Fig. 1b. In this case, the thickness of the mask itself minus the width of the final segment is 1.1 μm. Some much smaller features are visible in the vicinity of the nanowire, shown as secondary peaks in the line profile or small islands nearby in the AFM image. These are thought to be a combination of metal islands near the deposited structure and electronic defects created during the SEM imaging of the substrate. The aligned features running horizontally across the image are monatomic KBr steps decorated with metal islands. It is also possible to see the top of the half-shadow of the wire, where the wire size is actually decreased as a result of shadowing, see Fig. 1b. It is more difficult to precisely measure this distance due to the grain structure, but it is approximately 90–95 nm in width. This also agrees with the expected spreading of the incident evaporant beam.

4. Conclusion

We have demonstrated the creation of single crystal silicon membranes fabricated with a combination of standard micromachining and focussed ion beam milling. The use of robust silicon membranes considerably thicker than the typical silicon nitride stencils allows the simultaneous creation of 50 nm and several hundred micrometer sized features without compromising the membrane stability. Despite the lack of intrinsic stress and the inherent stiffness of these membranes, thick or highly stressed films will still pose an eventual problem. In order to compensate for this distortion we have introduced staircase structures into the local region of the membrane that still allow for small features but with minimal feature distortion under highly stressed films. Measurements of high stress metal films and calculated deflections of the modified structures agree and provide an effective method of membrane support for silicon stencils. The reinforced membranes have been used to deposit 180 nm structures on an insulating KBr surface in UHV where the deposited feature sizes agree with both the calculated and measured effects of the minimized membrane distortion due to the film deposition.

Acknowledgements

The authors would like to thank the staff of the McGill Nanotools Microfab for their support and useful discussions. We would

also like to thank the following funding agencies for their support: NSERC, CFI, Nano-Quebec, FQRNT, and CIFAR.

References

[1] M.M. Deshmukh, D.C. Ralph, M. Thomas, J. Silcox, Applied Physics Letters 75 (11) (1999) 1631–1633.
[2] J. Brugger, J.W. Berenschot, S. Kuiper, W. Nijdam, B. Otter, M. Elwenspoek, Microelectronic Engineering 53 (1–4) (2000) 403–405.
[3] G.M. Kim, M.A.F. van den Boogaart, J. Brugger, Microelectronic Engineering 67-8 (2003) 609–614.
[4] P. Zahl, M. Bammerlin, G. Meyer, R.R. Schlittler, Review of Scientific Instruments 76 (2) (2005) 023707.
[5] S. Egger, A. Ilie, Y.T. Fu, J. Chongsathien, D.J. Kang, M.E. Welland, Nano Letters 5 (1) (2005) 15–20.
[6] C. Gartner, R. Hoffman, F. Perez-Willard, M. Sauter, C. Surgers, H. Von Lohneysen, Review of Scientific Instruments 77 (2) (2006) 026101.
[7] R. Luthi, R.R. Schlittler, J. Brugger, P. Vettiger, M.E. Welland, J.K. Gimzewski, Applied Physics Letters 75 (9) (1999) 1314–1316.
[8] H.M. Guo, D. Martrou, T. Zambelli, J. Polesel-Maris, A. Piednoir, E. Dujardin, S. Gauthier, M.A.F. van den Boogaart, L.M. Doeswijk, J. Brugger, Applied Physics Letters 90 (9) (2007) 093113.
[9] V. Blech, T. Nobuyuki, B. Kim, Journal of Vacuum Science and Technology B 24 (1) (2006) 55–58.
[10] M.A.F. van den Boogaart, L.M. Doeswijk, J. Brugger, Journal of Microelectromechanical Systems 15 (6) (2006) 1663–1670.
[11] M.A.F. van den Boogaart, M. Lishchynska, L.M. Doeswijk, J.C. Greer, J. Brugger, Sensors and Actuators a-Physical 130 (2006) 568–574.
[12] M. Lishchynska, V. Bourenkov, M.A.F. van den Boogaart, L. Doeswijk, J. Brugger, J.C. Greer, Microelectronic Engineering 84 (1) (2007) 42–53.
[13] Z.W. Pan, S. Dai, D.B. Beach, D.H. Lowndes, Nano Letters 3 (9) (2003) 1279–1284.
[14] A. Linklater, J. Nogami, Nanotechnology 19 (28) (2008) 285302.
[15] G.G. Stoney, in: Proceedings of the Royal Society of London Series a-Containing Papers of a Mathematical and Physical Character 82 (553) (1909) 172–175.
[16] W.A. Brantley, Journal of Applied Physics 44 (1) (1973) 534–535.
[17] C.A. Klein, Journal of Applied Physics 88 (9) (2000) 5487–5489.
[18] R. Knepper, S.P. Baker, Applied Physics Letters 90 (18) (2007) 181908.
[19] G. Guisbiers, O. Van Overschelde, M. Wautelet, P. Leclere, R. Lazzaroni, Fractal dimension, Journal of Physics D – Applied Physics 40 (4) (2007) 1077–1079.